INTERNATIONAL JOURNAL FOR NUMERICAL METHODS IN FLUIDS, VOL. 26, 501–517 (1998)
Int. J. Numer. Meth. Fluids, **26**: 501–517 (1998).

A FAST ALGORITHM TO SOLVE VISCOUS TWO-PHASE FLOW IN AN AXISYMMETRIC ROCKET NOZZLE

R. C. MEHTA* AND T. JAYACHANDRAN
Aerodynamics Division, Vikram Sarabhai Space Centre, Trivandrum 695022, India

SUMMARY

A numerically fast algorithm has been developed to solve the viscous two-phase flow in an axisymmetric rocket nozzle. A Eulerian–Eulerian approach is employed in the computation to couple the gas–particle flow. Turbulence closure is achieved using a Baldwin–Lomax model. The numerical procedure employs a multistage time-stepping Runge–Kutta scheme in conjunction with a finite volume method and is made computationally fast for the axisymmetric nozzle. The present numerical scheme is applied to compute the flow field inside JPL and AGARD nozzles. © 1998 John Wiley & Sons, Ltd.

KEY WORDS: Multiphase; turbulent; finite volumes; structured grids; compressible flows

1. INTRODUCTION

Nozzle flow field analysis constitutes an important area of research and development work in aerospace engineering, since the performance of a launch vehicle depends on the propulsive power of the nozzle. Optimum thermal insulation of the nozzle wall also demands accurate estimation of the heat transfer rate to the nozzle wall. The aluminium oxide particles in the exhaust contribute to an inefficiency in the expansion process in the propulsive nozzle. This inefficiency is attributed to velocity and thermal lag between the gas and particles. It is necessary to know the behaviour of the two-phase flow expanding through the nozzle in order to evaluate the motor performance.

Since the 1970s, numerical simulation of the gas–particle two-phase nozzle has been extensively studied with the development of numerical schemes. Chang[1] has solved the unsteady two-fluid equations in conservation form using MacCormack's scheme to predict the gas and particle fields in an axisymmetric convergent–divergent nozzle. Crowe[2] provides a review of numerical models for dilute gas–particle flows. The main advantage of the two fluid model is that the numerical procedures already established for single-phase flow can be used for two-phase flow. However, the major drawbacks of this scheme are numerical diffusion of the particle phase and higher computer storage and computer time requirements for multisize particles. A numerical study of the gas–particle flow in a solid motor nozzle has been made by Hwang and Chang[3] using MacCormack's explicit scheme in

---

* Correspondence to: R. C. Mehta, Aerodynamics Division, Vikram Sarabhai Space Centre, Trivandrum 695022, India

CCC 0271–2091/98/050501–17 $17.50

Received March 1996
Revised March 1997

conjunction with a trajectory model. Nishida and Ishimaru[4] have obtained the numerical simulation of gas–solid two-phase non-equilibrium nozzle flows using MacCormack's scheme with TVD (total variation diminishing). This numerical scheme needs extra computer time to compute explicit characteristic flux difference and Jacobian terms.

The objective of the present work is to develop a fast numerical algorithm to solve the two-phase viscous flow in an axisymmetric convergent–divergent nozzle, employing a simple structured grid arrangement. A time-dependent numerical scheme in conjunction with a finite volume discretization is developed for solution of the two-phase viscous flow in the axisymmetric nozzle. An algebraic turbulence model[5] is used to compute the eddy viscosity. A Eulerian–Eulerian approach with appropriate exchange terms for gas–particle interaction is used for formulation of the equations. Since the number of equations is increased as compared with inviscid flow, the numerical simulation demands a considerable amount of computer CPU time to obtain a converged solution. A reduction in CPU time is achieved by using a special structured grid arrangement in the numerical discretization. The fast numerical algorithm has been tested and validated on the well-documented JPL and AGARD nozzles in order to demonstrate the performance and versatility of the code. The ideas contained in the proposed fast numerical algorithm can easily be extended to analyse the performance of an air breathing rocket nozzle where the fluid dynamics equations are coupled with a two-phase, two-equation turbulence model and finite rate chemistry.

2. ANALYSIS

The governing equations for gas flow are the time-dependent axisymmetric compressible Navier–Stokes equations in weak conservation form. For two-phase flow the governing equations are written in the Eulerian–Eulerian formulation

$$\frac{\partial \mathbf{W}}{\partial t} + \frac{\partial \mathbf{F}}{\partial x} + \frac{\partial \mathbf{G}}{\partial \mathbf{r}} + \mathbf{H} = \frac{\partial \mathbf{R}}{\partial x} + \frac{\partial \mathbf{S}}{\partial \mathbf{r}}, \tag{1}$$

where **W** is the solution vector and **F** and **G** are the convective fluxes:

$$\mathbf{W} = r\begin{bmatrix} \rho \\ \rho u \\ \rho v \\ \rho e \\ \rho_{\mathrm{P}} \\ \rho u_p \\ \rho v_{\mathrm{P}} \\ \rho E_{\mathrm{P}} \end{bmatrix}, \qquad \mathbf{F} = r\begin{bmatrix} \rho u \\ \rho u^2 + p \\ \rho uv \\ u(\rho e + p) \\ \rho_{\mathrm{P}} u_{\mathrm{P}} \\ \rho_{\mathrm{P}} u_{\mathrm{P}}^2 \\ \rho_{\mathrm{P}} u_{\mathrm{P}} v_{\mathrm{P}} \\ \rho_{\mathrm{P}} u_{\mathrm{P}} E_{\mathrm{P}} \end{bmatrix}, \qquad \mathbf{G} = r\begin{bmatrix} \rho v \\ \rho uv \\ \rho v^2 + p \\ v(\rho e + p) \\ \rho_{\mathrm{P}} v_{\mathrm{P}} \\ \rho_{\mathrm{P}} v_{\mathrm{P}} u_{\mathrm{P}} \\ \rho_{\mathrm{P}} v_{\mathrm{P}}^2 \\ \rho_{\mathrm{P}} v_{\mathrm{P}} E_{\mathrm{P}} \end{bmatrix}.$$

The viscous fluxes **R** and **S** and the source term **H** are written as

$$\mathbf{R} = r\begin{bmatrix} 0 \\ \sigma_{xx} \\ \sigma_{xr} \\ u\sigma_{xx} + v\sigma_{xr} - q_x \\ 0 \\ 0 \\ 0 \\ 0 \end{bmatrix}, \qquad \mathbf{S} = r\begin{bmatrix} 0 \\ \sigma_{xr} \\ \sigma_{rr} \\ u\sigma_{xr} + v\sigma_{rr} - q_r \\ 0 \\ 0 \\ 0 \\ 0 \end{bmatrix}, \qquad \mathbf{H} = \begin{bmatrix} 0 \\ A \\ B + (p + \sigma_{\theta\theta}) \\ C \\ 0 \\ -A \\ -B \\ -C \end{bmatrix},$$

where σ represents the stress vector and q the heat flux vector, which are given by the constitutive equations for a Newtonian fluid:

$$\begin{aligned}
\sigma_{xx} &= -\frac{2}{3}(\mu+\mu_t)\left(\frac{\partial u}{\partial x}+\frac{\partial v}{\partial r}+\frac{v}{r}\right)+2(\mu+\mu_t)\frac{\partial u}{\partial x},\\
\sigma_{rr} &= -\frac{2}{3}(\mu+\mu_t)\left(\frac{\partial u}{\partial x}+\frac{\partial v}{\partial r}+\frac{v}{r}\right)+2(\mu+\mu_t)\frac{\partial v}{\partial r},\\
\sigma_{xr} &= -(\mu+\mu_t)\left(\frac{\partial u}{\partial r}+\frac{\partial v}{\partial x}\right),\\
\sigma_{\theta\theta} &= -\frac{2}{3}(\mu+\mu_t)\left(\frac{\partial u}{\partial x}+\frac{\partial v}{\partial r}+\frac{v}{r}\right)+2(\mu+\mu_t)\frac{v}{r},\\
q_x &= C_P\left(\frac{\mu}{Pr}+\frac{\mu_t}{Pr_t}\right)\frac{\partial T}{\partial x}, \qquad q_r = C_P\left(\frac{\mu}{Pr}+\frac{\mu_t}{Pr_t}\right)\frac{\partial T}{\partial r},\\
E_P &= C_{PP}T_P+\tfrac{1}{2}(u_P^2+v_P^2).
\end{aligned}$$

Where Pr and Pr_t, the laminar and turbulent Prandtl numbers, are assumed to take constant values of 0·72 and 0·9 respectively. The coefficient of molecular viscosity is calculated according to Sutherland's law. The pressure p can be obtained from the equation of state of a perfect gas:

$$p=\rho(\gamma-1)[e-0{\cdot}5(u^2+v^2)]. \tag{2}$$

3. TURBULENCE MODEL

In the present investigation a two-layer algebraic model[5] has been used for turbulence closure. This model, which utilizes the vorticity distribution to determine the scale lengths, has been used previously and is reputed to yield acceptable engineering solutions.[6]

In the inner region the eddy viscosity is given by

$$(\mu_t)_i=(0{\cdot}4D_1L)\rho|\omega|, \tag{3}$$

where ω is the vorticity function, L is the normal distance to the nozzle wall and D_1 is Van Driest's damping factor:

$$D_1=1-\exp\left[-\left(\frac{\rho_w|\omega|_w}{\mu_w}\right)^{0{\cdot}5}\frac{L}{26}\right]. \tag{4}$$

In the outer region,

$$(\mu_t)_o=0{\cdot}0168\ (1{\cdot}6)F_wF_{KIF.} \tag{5}$$

The coefficient F_w is calculated as the minimum of the following two values:

(i) $L_{max}F_{max}$, (ii) $0{\cdot}25\mathrm{L}_{max}\max[(\mathrm{u}^2+v^2)]^{0{\cdot}5}/\mathrm{F}_{max}$.

The scale length L_{max} is the maximum value of L when the function $F\ (=LD_1|\omega|)$ attains its maximum F_{max}. The Klebanoff intermittency correction factor is given by

$$F_{KIF}=\left[1+5{\cdot}5\left(0{\cdot}3\frac{L}{L_{max}}\right)^6\right]^{-1}. \tag{6}$$

The effective viscosity is then given by

$$\mu_t = \min(\mu_i, \mu_o). \tag{7}$$

4. GAS–PARTICLE INTERACTIONS

The coupling between gas and particle phases is made through the exchange of mass, momentum and energy at the interface. In the present analysis the burning of particles is neglected and hence the mass exchange is zero. The terms A and B represent the momentum exchange and C represents the energy exchange. The coupling between phases is included through the source terms A, B and C in the gas phase conservation equations and $-A$, $-B$ and $-C$ in the particle phase conservation equations. The force exerted on a single particle moving through a gas is given as[7]

$$F_P = 6\pi r_P f_D (u - u_P), \tag{8}$$

so that for N particles in a unit volume the effective drag force is

$$A = N6\pi r_P f_D \mu (u - u_P), \tag{9}$$

$$B = N6\pi r_P f_D \mu (v - v_P), \tag{10}$$

where f_D is the ratio of the drag coefficient C_D to the Stokes drag $C_{D0} = 24/Re_P$ and is given by[8]

$$f_D = 1 + 0{\cdot}33 Re_P^{0{\cdot}65}. \tag{11}$$

Where the Reynolds number Re_P based on the relative velocity between gas and particle phases is

$$Re_P = 2|\Delta q_P| r_P \rho/\mu, \tag{12}$$

with

$$|\Delta q_P| = [(u - u_P)^2 + (v - v_P)^2]^{0{\cdot}5}. \tag{13}$$

The heat transferred from gas to particle phase per unit volume is given as[1]

$$Q_P = N2\pi r_P \lambda Nu (T - T_P), \tag{14}$$

where λ is the thermal conductivity of the gas and Nu, the Nusselt number, is written as[1]

$$Nu = 2{\cdot}0 + 0{\cdot}459 Re_P^{0{\cdot}55} Pr^{0{\cdot}33}. \tag{15}$$

The gas–particle energy term is given by

$$C = u_P A + v_P B + Q_P, \tag{16}$$

where the first two terms on the right-hand side represent the energy exchange due to momentum transfer.

5. BOUNDARY CONDITIONS

Four types of boundary conditions are required for the computation of the flow field, i.e. wall, inflow, outflow and symmetry conditions. They are prescribed as follows.

On the impermeable wall, no-slip conditions are specified along with an adiabatic wall for both gas and particle phases.

A the subsonic inflow the stagnation pressure and temperature are specified. The axial velocity u is extrapolated. The radial velocity v is calculated from the inlet flow angle. Other variables are calculated assuming 1% lag and the particle density using the specific loading ϕ.

For the supersonic outflow case all quantities are linearly extrapolated at the outflow from the vector of conserved variables **W** as

$$\mathbf{W}_{nx,j} = 2\mathbf{W}_{nx-1,j} - \mathbf{W}_{nx-2,j}, \tag{17}$$

where the subscript nx represents the last grid point on the boundary.

On the centreline of the axisymmetric nozzle the normal velocities of gas and particle phases and the gradients in the normal direction of all other variables are specified as zero.

6. STRUCTURED GRID

A structured finite volume grid system consisting of quadrilateral cells is generated using a simple algebraic relation in conjunction with the given nozzle geometry. The nozzle centreline is divided judiciously into a number of non-uniformly spaced grid points, taking into consideration the local flow conditions. The normal grid points are generated perpendicular to the nozzle axis. In order to insure a proper resolution of the boundary layer in the vicinity of the nozzle wall, the normal direction grid points are exponentially stretched using the relation

$$r_{i,j} = Rn\frac{\exp(-\beta j/nr) - 1}{\exp(\beta) - 1}, \tag{18}$$

where Rn is the local radius of the nozzle at station i and β is a stretching factor. The values of i and j vary from 1 to nx and from 1 to nr respectively. It is important to mention here that the structured grid arrangement is well suited for the algebraic turbulence model.

7. NUMERICAL SCHEME

To facilitate the finite volume spatial discretization in the computation method, the equations of motion of the fluid can be written in the integral form

$$\frac{\partial}{\partial t}\int_{\Omega} \mathbf{W}\, \mathrm{d}\Omega + \int_{\Gamma} (\mathbf{F}\, \mathrm{d}r - \mathbf{G}\, \mathrm{d}x) = \int_{\Gamma} (\mathbf{R}\, \mathrm{d}r - \mathbf{S}\, \mathrm{d}x) - \int_{\Omega} \mathbf{H}\, \mathrm{d}\Omega, \tag{19}$$

where Ω is the computational domain and Γ is the boundary of the domain. The contour integration around the boundary of the cell is taken in the anticlockwise sense.

The computational domain is divided into a finite number of non-overlapping quadrilateral cells. Figure 1 depicts a typical cell which has four edges $(1, 2, 3, 4)$ and four vertices (A, B, C, D). The conservative variables within the computational cell are represented by their average values at the cell centre P. When the integral governing equations (19) are applied separately to each cell in the domain, we obtain a set of coupled ordinary differential equations of the form

$$A_{ij}\frac{\partial \mathbf{W}_{i,j}}{\partial t} + \mathbf{Q}(\mathbf{W}_{i,j}) - \mathbf{V}(\mathbf{W}_{i,j}) - A_{i,j}\mathbf{H}_{i,j} = 0, \tag{20}$$

where $\mathbf{Q}(\mathbf{W}_{i,j})$ and $\mathbf{V}(\mathbf{W}_{i,j})$ are the inviscid and viscous fluxes respectively.

7.1. Inviscid terms

The convective fluxes are calculated at the centre, resulting in cell-centre flux balances. The contour integration of the inviscid flux vector is approximated as

$$\mathbf{Q}(\mathbf{W}_{i,j}) = \sum_{s=1}^{4}(\mathbf{F}_s\Delta r_s - \mathbf{G}_s\Delta x_s). \tag{21}$$

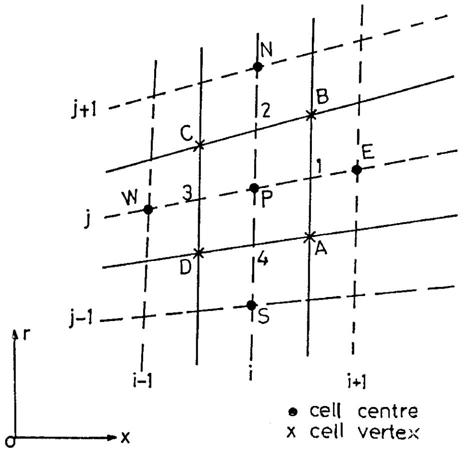

Figure 1. Computational cell

The summation is done over the four edges of the cell as depicted in Figure 1 and can be simplified as

$$\mathbf{Q}(\mathbf{W}_{i,j}) = \mathbf{F}_{\mathrm{AB}}\Delta r_{\mathrm{AB}} + \mathbf{F}_{\mathrm{BC}}\Delta r_{\mathrm{BC}} + \mathbf{F}_{\mathrm{CD}}\Delta r_{\mathrm{CD}} + F_{\mathrm{DA}}\Delta r_{\mathrm{DA}} - \mathbf{G}_{\mathrm{BC}}\Delta x_{\mathrm{BC}} - \mathbf{G}_{\mathrm{DA}}\Delta x_{\mathrm{DA}}, \tag{22}$$

where $\Delta x_{\mathrm{BC}} = X_{\mathrm{B}} - X_{\mathrm{C}}$, $\Delta r_{\mathrm{AB}} = r_{\mathrm{A}} - r_{\mathrm{B}}$, etc. are incremental distances. The terms Δx_{AB} and Δx_{CD} are zero, because the grid lines are perpendicular to the axis. Cell-edge values of the inviscid flux terms are approximated by the average of two adjacent cell-centre values, e.g.

$$\mathbf{F}_{\mathrm{AB}} = 0{\cdot}5(\mathbf{F}_{i,j} + \mathbf{F}_{i+1,j}).$$

7.2. Viscous terms

The viscous terms are defined at the centre of the cell. The above procedure is repeated to approximate the contour integration of the viscous flux vector as

$$\mathbf{V}(\mathbf{W}_{i,j}) = \sum_{s=1}^{4}(\mathbf{R}_s\Delta r_s - \mathbf{S}_s\Delta x_s).$$

The inclusion of diffusion transport requires a choice of the locations at which the diffusive fluxes are evaluated and the volume over which their derivatives should be integrated. The derivatives $\partial f/\partial x$ and $\partial f/\partial r$ at the cell vertices (A, B, C, D) can be determined by considering auxiliary cells surrounding each side as depicted in Figure 1, where f stands for any of the flow variables u, v or T. The viscous flux vectors **R** and **S** are approximated in such a way as to preserve cell conservation and maintain algorithm simplicity. The derivatives of f at the vertices of the cell are evaluated by discrete application of the divergence theorem[9] to the auxiliary cell as

$$A'_{\mathrm{AB}}\left.\frac{\partial f}{\partial x}\right|_{\mathrm{AB}} = [(f_{\mathrm{E}} - f_{\mathrm{P}})\Delta r_{\mathrm{AB}} + (f_{\mathrm{B}} - f_{\mathrm{A}})\Delta r_{\mathrm{PE}}], \tag{23a}$$

$$A'_{\mathrm{BC}}\left.\frac{\partial f}{\partial x}\right|_{\mathrm{BC}} = [(f_{\mathrm{B}} - f_{\mathrm{C}})\Delta r_{\mathrm{PN}} + (f_{\mathrm{N}} - f_{\mathrm{P}})\Delta r_{\mathrm{BC}}], \tag{23b}$$

$$A'_{\mathrm{CD}}\left.\frac{\partial f}{\partial x}\right|_{\mathrm{CD}} = [(f_{\mathrm{P}} - f_{\mathrm{W}})\Delta r_{\mathrm{CD}} + (f_{\mathrm{C}} - f_{\mathrm{D}})\Delta r_{\mathrm{PW}}], \tag{23c}$$

$$A'_{\mathrm{DA}}\left.\frac{\partial f}{\partial x}\right|_{\mathrm{DA}} = [(f_{\mathrm{A}} - f_{\mathrm{D}})\Delta r_{\mathrm{PS}} + (f_{\mathrm{P}} - f_{\mathrm{S}})\Delta r_{\mathrm{DA}}], \tag{23d}$$

where A' is the area of the secondary cell. In a similar way the derivative of f in the other co-ordinate direction can be written as

$$A'_{\mathrm{AB}}\left.\frac{\partial f}{\partial r}\right|_{\mathrm{AB}} = (f_{\mathrm{B}} - f_{\mathrm{A}})\Delta x_{\mathrm{PE}}, \tag{24a}$$

$$A'_{\mathrm{BC}}\left.\frac{\partial f}{\partial r}\right|_{\mathrm{BC}} = (f_{\mathrm{N}} - f_{\mathrm{P}})\Delta x_{\mathrm{BC}}, \tag{24b}$$

$$A'_{\mathrm{CD}}\left.\frac{\partial f}{\partial r}\right|_{\mathrm{CD}} = (f_{\mathrm{C}} - f_{\mathrm{D}})\Delta x_{\mathrm{PW}}, \tag{24c}$$

$$A'_{\mathrm{DA}}\left.\frac{\partial f}{\partial r}\right|_{\mathrm{DA}} = (f_{\mathrm{P}} - f_{\mathrm{S}})\Delta x_{\mathrm{DA}}. \tag{24d}$$

The terms Δx_{AB}, Δx_{CD}, Δx_{PN} and Δx_{PS} again become zero, because the grid lines are again perpendicular to the axis.

On sufficiently smooth grids the above finite volume discretization is second-order-accurate.

7.3. Artificial dissipation

In cell-centre spatial discretization schemes, such as the one described above which is non-dissipative, where numerical errors (truncation, round-off, etc.) are not damped in time, oscillations may be present in the steady state solution. In order to eliminate these oscillations, artificial dissipative terms are added to (20), which now becomes

$$\bar{r}_{\mathrm{c}} A_{i,j}\frac{\mathrm{d}\mathbf{W}_{i,j}}{\mathrm{d}t} = -[\mathbf{Q}(\mathbf{W}_{i,j}) - \mathbf{V}(\mathbf{W}_{i,j}) - \mathbf{D}(\mathbf{W}_{i,j})] + A_{i,j}\mathbf{H}(\mathbf{W}_{i,j}). \tag{25}$$

The approach of Jameson *et al.*[10] is adopted to construct the dissipative function $D_{i,j}$ consisting of a blend of second and fourth differences of the vector of conserved variables $\mathbf{W}_{i,j}$. Fourth differences are added everywhere in the flow domain where the solution is smooth, but are 'switched off' in the region of shock waves. A term involving second differences is then 'switched on' to damp oscillations near shock waves. This switching is achieved by means of a shock wave sensor based on the local second differences of pressure. Since the computational domain is structured, the cell centres are defined by the two indices (i, j) in these co-ordinate directions. The dissipation terms are written in terms of differences of cell-edge values as

$$D_{i,j} = (d_{\mathrm{AB}} - d_{\mathrm{CD}} + d_{\mathrm{BC}} - d_{\mathrm{DA}})/\Delta A_{i,j}, \tag{26}$$

where $\Delta A_{i,j}$ is the local cell-centre time step. The cell-edge components of the artificial dissipation are composed of first and third differences of the dependent variables, e.g.

$$d_{\mathrm{AB}} = (d^{(2)}_{\mathrm{AB}} - d^{(4)}_{\mathrm{AB}})\left(\frac{\Delta t_{i,j}}{2\Delta A_{i,j}} + \frac{\Delta t_{i+1,j}}{2\Delta A_{i+1,j}}\right), \tag{27}$$

with

$$d^{(2)}_{\mathrm{AB}} = \epsilon^{(2)}_2(\mathbf{W}_{i+1,j} - \mathbf{W}_{i,j}), \qquad d^{(4)}_{\mathrm{AB}} = \epsilon^{(4)}_2(\mathbf{W}_{i+2,j} - 3\mathbf{W}_{i+1,j} + 3\mathbf{W}_{i,j} - \mathbf{W}_{i-1,j}).$$

The adaptive coefficients

$$\epsilon^{(2)}_2 = \kappa^{(2)}\max(v_{i+1,j}, v_{i,j}), \qquad \epsilon^{(4)}_2 = \max(0, \kappa^{(4)} - \epsilon^{(2)}_2) \tag{28}$$

are switched on or off by use of the shock wave sensor v, with

$$v_{i,j} = \left|\frac{p_{i+1,j} - 2p_{i,j} + p_{i-1,j}}{p_{i+1,j} + 2p_{i,j} + p_{i-1,j}}\right|, \tag{29}$$

where $\kappa^{(2)}$ and $\kappa^{(4)}$ are constants, taken equal to 1·0 and 0·03125 respectively in the above calculations. The blend of second and fourth differences provides third-order background dissipation in smooth regions of the flow and first-order dissipation at shock waves.

7.4. Time-marching scheme

The spatial discretization described above reduces the governing flow equations to semidiscrete ordinary differential equations. The integration is performed using an efficient multistage scheme.[10] Since time accuracy is not important for a steady state solution, such schemes are selected only for their properties of stability and damping. The following three-stage, time-stepping method is adopted for the present work (neglecting for clarity the subscripts i and j).

$$\begin{aligned}
\mathbf{W}^{(0)} &= \mathbf{W}^{n},\\
\mathbf{W}^{(1)} &= \mathbf{W}^{(0)} - (0{\cdot}6\Delta t/\Delta A)(\mathbf{R}^{(0)} - \mathbf{D}^{(0)}),\\
\mathbf{W}^{(2)} &= \mathbf{W}^{(0)} - (0{\cdot}6\Delta t/\Delta A)(\mathbf{R}^{(1)} - \mathbf{D}^{(0)}),\\
\mathbf{W}^{(3)} &= \mathbf{W}^{(0)} - (1{\cdot}0\Delta t/\Delta A)(\mathbf{R}^{(2)} - \mathbf{D}^{(0)},\\
\mathbf{W}^{n+1} &= \mathbf{W}^{(3)},
\end{aligned} \tag{30}$$

where n is the current time level, $n+1$ is the new time level and $\mathbf{R}$ is the sum of inviscid and viscous fluxes. The temporal accuracy of (30) is third-order.[10] In order to minimize the computational time, the expensive evaluation of the dissipation function $\mathbf{D}$ is carried out only at the first intermediate stage (0) and then frozen for the subsequent stages. This is known to modify the stability criterion of the scheme, but the steady state accuracy and convergence characteristics are preserved. The numerical scheme is stable for a Courant number $\leqslant 2$. Local time steps are used to accelerate convergence to a steady state solution, advancing the time step at each grid point by the maximum permissible amount allowed by the local CFL condition.

8. RESULTS AND DISCUSSION

The fast numerical algorithm developed above is applied to solve viscous two-phase flow. The inviscid flow results are taken as initial guess for the viscous flow. The reduction of CPU time for

Table I. Nozzle data

	JPL nozzle	AGARD nozzle
$(\Delta x)_{\min}$ (m)	0·0017	0·0011
$(\Delta x)_{\max}$ (m)	0·005	0·0064
$(\Delta r)_{\min}$ (m)	0·0008	0·0002
$(\Delta r)_{\max}$ (m)	0·0028	0·0024

evaluation of the flux terms can be seen by examining equations (22) and (24). The present algorithm takes about 25% less CPU time/cell/iteration/time step for computation of the inviscid terms. In the computation of the radial direction flux quantities the computer code saves about 50% CPU time for each cell/iteration/time step. All computations are performed on a Landmark I860-based workstation using double-precision arithmetic and an optimum compiler. Numerical computations are presented here for the well-documented axisymmetric JPL and AGARD nozzles. Grid independence tests are carried out taking into consideration the number of grid points in the axial and radial directions and the stretching factor to control the grid density near the nozzle wall. The grid size used for the JPL nozzle gives a relative difference or about ±2% in the nozzle wall and centreline pressure distribution, while for the AGARD nozzle the error in the computation of the specific impulse is about $-0{\cdot}4\%$. The minimum and maximum values of Δx and Δr in the convergent and divergent regions of the nozzle are given in Table I.

8.1. JPL nozzle (single-phase)

First of all, single-phase calculations were carried out. Figure 2(a) shows the JPL nozzle configuration. As shown in Figure 2(b), the computational domain of the nozzle is divided into a structured grid of 42×32 nodes. The chamber pressure and temperature are given in Table II. The calculated pressure ratio (p/P_0) variations along the wall and centreline are shown in Figure 3 along with the JPL test data.[11] The agreement between the results of this study and the experimental data is very good in the entire flow region. This shows that good resolution of the boundary flow variables is obtained using the simple structured grid arrangement.

8.2. JPL nozzle (two-phase)

The algorithm is now applied to a viscous two-phase flow problem. The chamber conditions are the same as in the single-phase flow case. The density, specific heat, particle size and particle mass loading are given in Table II. The inviscid flow results are taken as starting solution for the two-phase flow. Figures 4–7 show the Mach and particle contours for 3 and 5 μm radius aluminium oxide particles. It can be observed from the figures that as the particle size increases, the particle shift from the nozzle wall in the divergent area of the nozzle. The particle number density contours show interesting flow features of the two-phase flow. The maximum particle density is found on the wall upstream of the throat. A sharp change in particle density is found near the upper wall downstream of the throat, where the particle density drastically decreases to a small value. Figure 8 shows the centreline variation of Mach number and gas temperature. It can be seen from the figures that as the particle size increases, the Mach number and gas temperature decrease along the centreline of the nozzle.

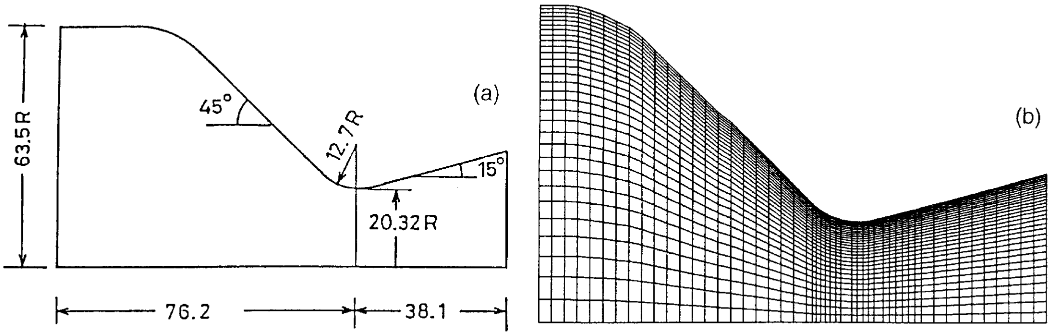

Figure 2. (a) Schematic sketch of JPL nozzle. (b) Grid for JPL nozzle

Table II. Two-phase flow input data for JPL nozzle

Gas phase	Particle phase
$P_0 = 1{\cdot}0342\,\text{MPa}$	$C_{\text{PP}} = 1380{\cdot}0\,\text{J}\,\text{kg}^{-1}\,\text{K}^{-1}$
$T_0 = 555{\cdot}0\,\text{K}$	$\rho_p = 4004{\cdot}62\,\text{kg}\,\text{m}^{-3}$
$\gamma = 1{\cdot}4$	$r_p = 3$ and $5\,\mu\text{m}$
$C_{\text{P}} = 1070{\cdot}0\,\text{J}\,\text{kg}^{-1}\,\text{K}^{-1}$	$\phi = 0{\cdot}3$
$Pr = 0{\cdot}74$	

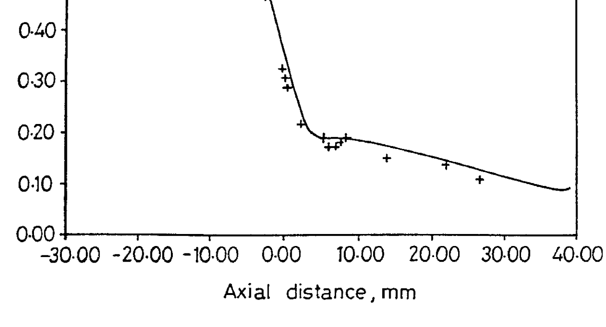

Figure 3(a). Wall pressure distribution for JPL nozzle flow

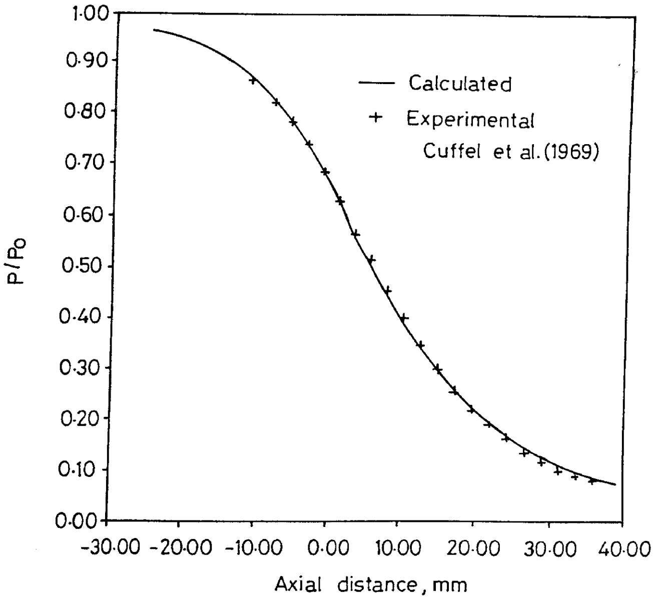

Figure 3(b). Centreline pressure distribution for JPL nozzle flow

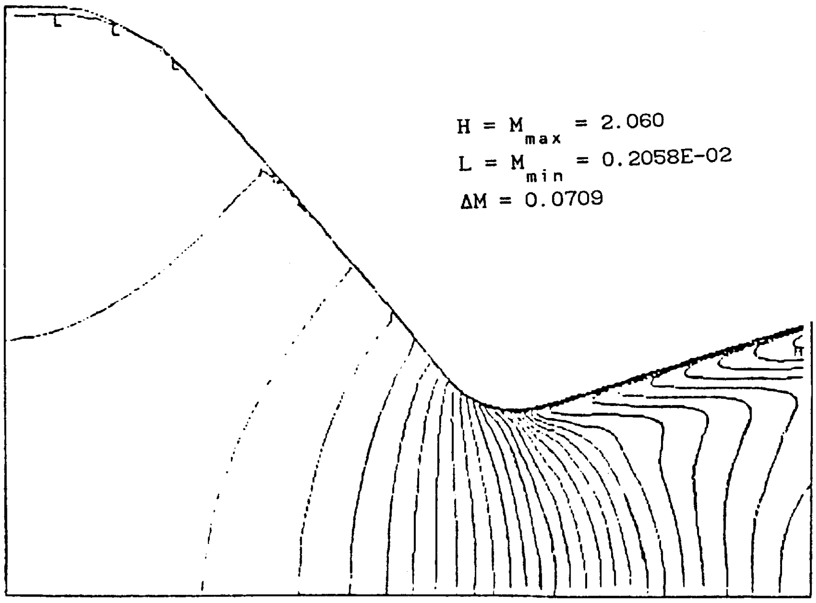

Figure 4. Iso-Mach contours for two-phase JPL nozzle flow ($r_P = 3\,\mu m$)

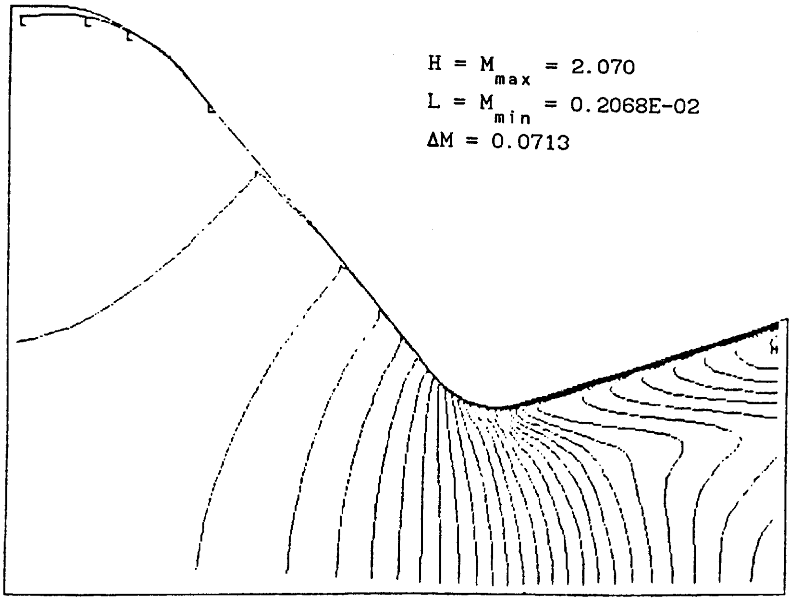

Figure 5. Iso-Mach contours for two-phase JPL nozzle flow ($r_P = 5\ \mu m$)

8.3. AGARD-nozzle

The propellant composition, operating conditions and nozzle configuration are as follows for the AGARD nozzle: ammonium perchlorate 68%, aluminium 20%, binder 12%, average chamber pressure 7·3 MPa, throat radius 41 mm, area ratio 60, initial angle 29·8°, exit angle 15°. Using these inputs, we calculated the following: stagnation temperature 3618·0 K, specific heat ratio 1·249, Prandtl number 0·3368, gas molecular weight 20·42, mass fraction 0·315. Figure 9 shows the grid

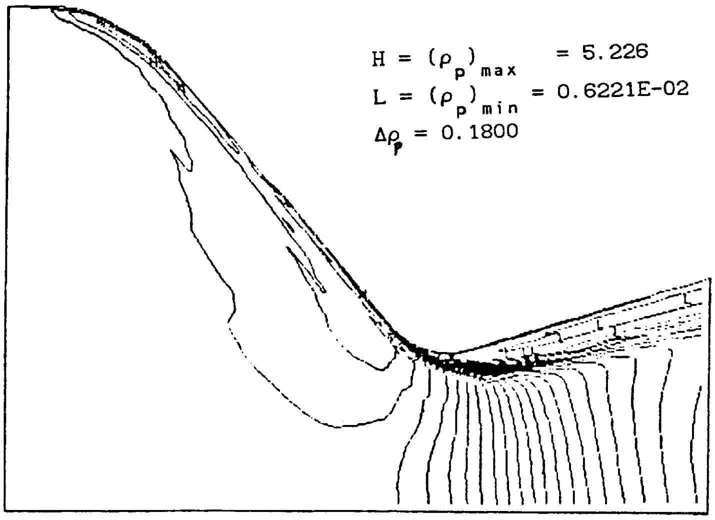

Figure 6. Particle number density contours ($r_P = 3\ \mu m$)

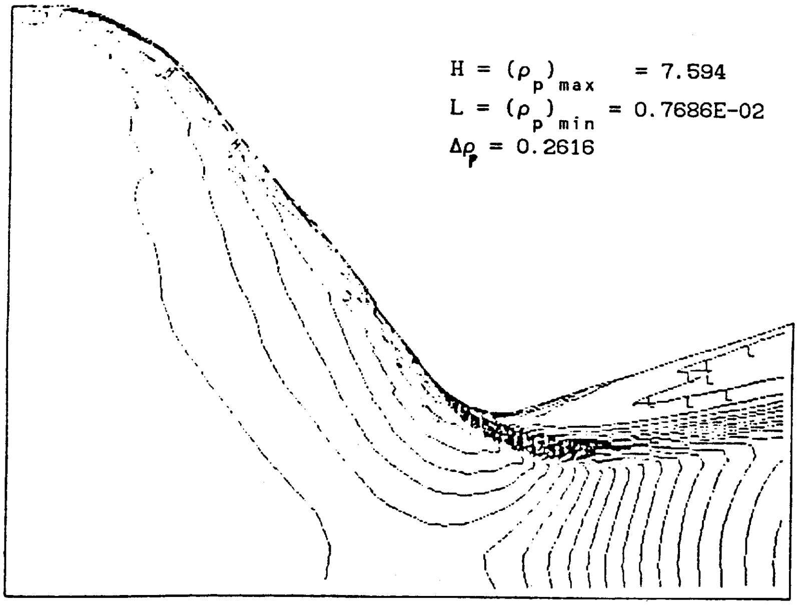

Figure 7. Particle number density contours ($r_P = 5\,\mu m$)

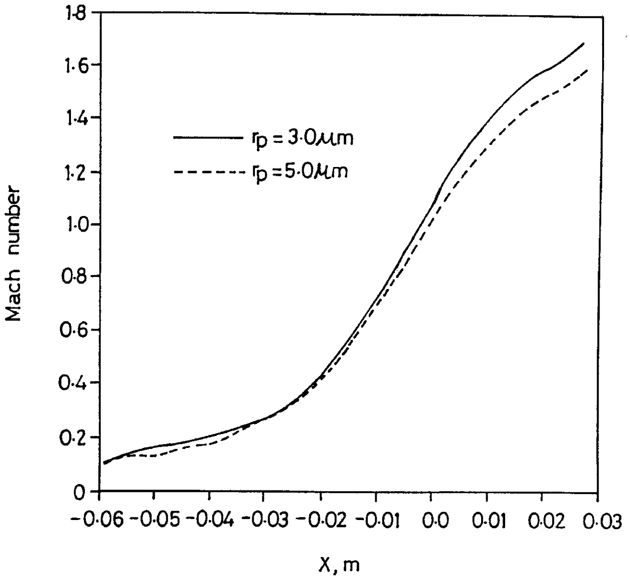

Figure 8(a). Variation of Mach number along centreline

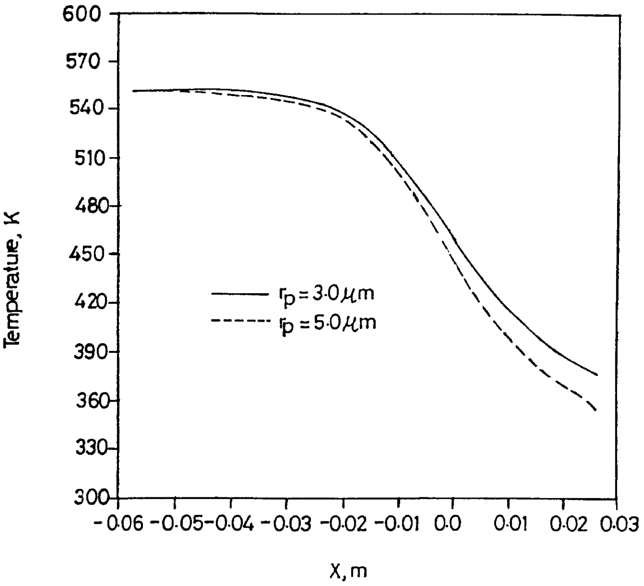

Figure 8(b). Variation of gas temperature along centreline

distribution inside the AGARD nozzle (90 × 60). Figure 10 displays the vector plot for a particle radius of 1 μm. Figure 11 shows the Mach and particle contours. The particles are separated from the nozzle wall in the downstream region of the throat and create a particle-free zone. The specific impulse of the AGARD nozzle for 1 μm radius particles is calculated as 295·6 s, which is close to the measured value of 296·7 s. The error in the specific impulse prediction is — 0·4%. This shows that a prediction accuracy of less than 1.0% can be achieved by the numerical simulation. It is worth mentioning here that the specific impulse of the propulsive nozzle is an important requirement for the mission simulation of a launch vehicle.

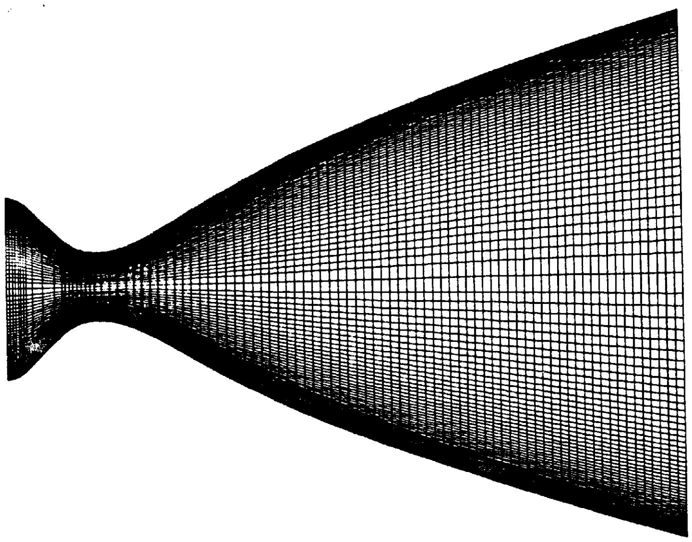

Figure 9. Grid for AGARD nozzle

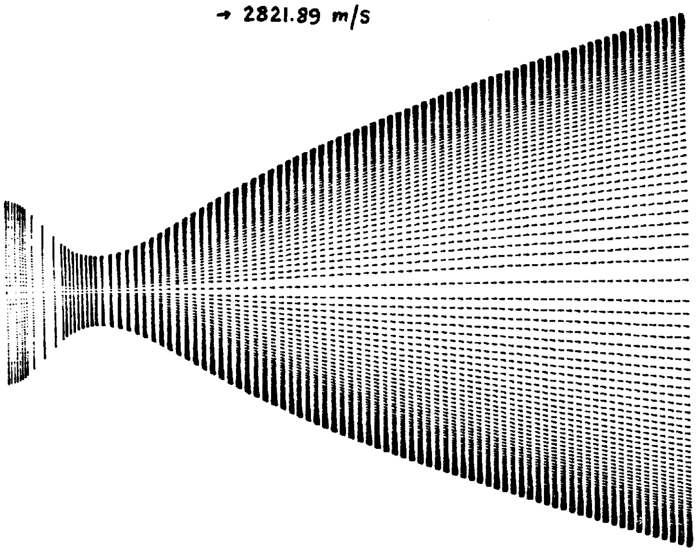

Figure 10. Vector plot ($r_P = 1$ μm)

9. CONCLUSIONS

A computationally fast algorithm is developed to solve compressible unsteady viscous two-phase flow in the axisymmetric nozzle. A structured grid arrangement is employed for numerical discretization. The grid is normal to the axial direction, which reduces the number of terms in the summation of inviscid and viscous fluxes. The grid is very convenient for the algebraic turbulence

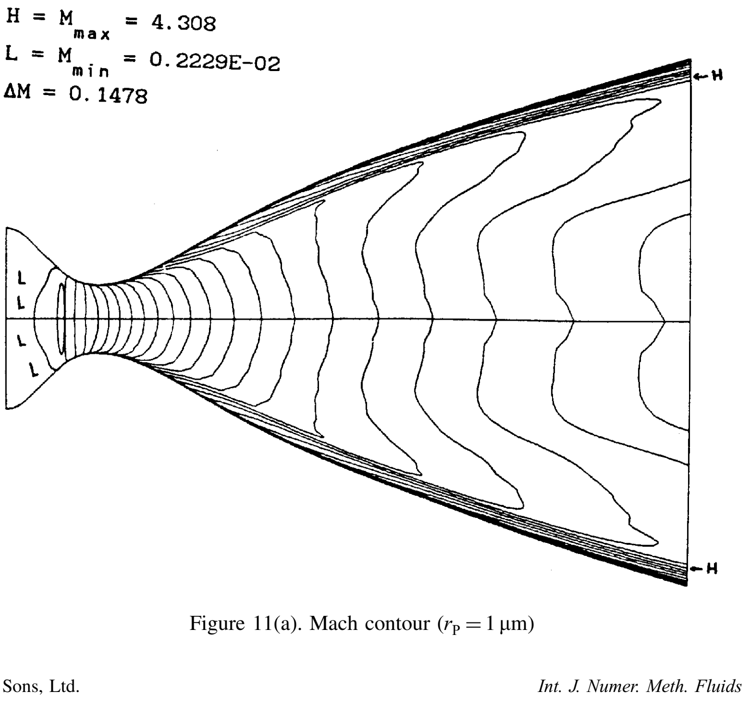

Figure 11(a). Mach contour ($r_P = 1$ μm)

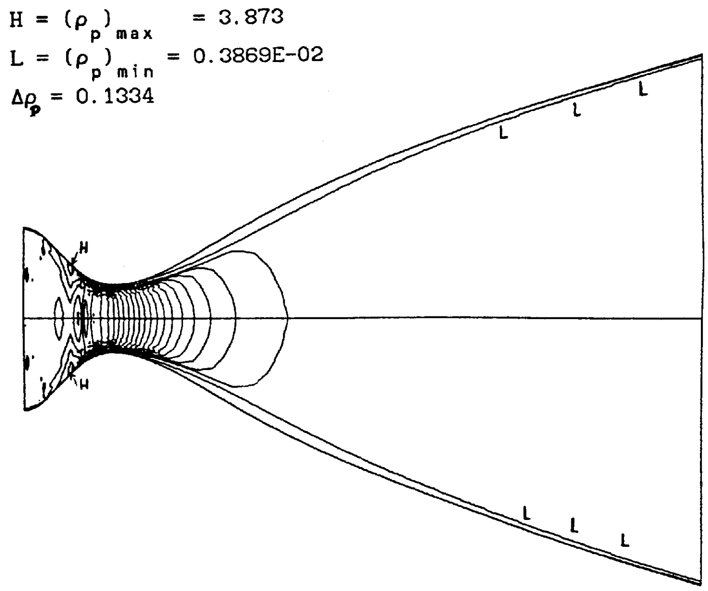

Figure 11(b). Particle density contours ($r_P = 1\ \mu m$)

model. A multistage, explicit, time-marching scheme is used to simulate numerically the flow field inside the axisymmetric nozzle. The effects of particle size on the flow field are investigated for JPL and AGARD nozzles.

APPENDIX: NOMENCLATURE

C_P	specific heat at constant pressure
C_{PP}	specific heat of particle phase
e	specific energy
E_P	enthalpy of particle phase
f_D	drag
$\mathbf{E}, \mathbf{F}, \mathbf{H}$	flux vectors
M	Mach number
N	particles in a unit volume
p	static pressure
P_0	stagnation pressure
Pr	Prandtl number
q	heat flux
t	time
T	temperature
u, v	velocity components
$\mathbf{W}$	conservative vector
x, r	polar co-ordinates

Greek letters

γ	ratio of specific heats
μ	molecular viscosity
ρ	density
σ	stress
ϕ	particle specific loading
ω	vorticity

Subscripts

p	particle
0	stagnation

REFERENCES

1. I. S. Chang, 'One- and two-phase nozzle flows', *AIAA J.*, **18**, 1455–1461 (1980).
2. C. T. Crowe, 'Numerical models for dilute gas–particle flows', *J. Fluids Engng.*, **104**, 297–303 (1982).
3. C. J. Hwang and G. C. Chang, 'Numerical study of gas–particle flow in a solid rocket nozzle', *AIAA J.*, **26**, 682–689 (1988).
4. M. Nishida and S. Ishimaru, 'Numerical analysis of gas–solid two-phase nonequilibrium nozzle flows', *JSME*, **33**, 494–599 (1990).
5. B. S. Baldwin and H. Lomax, 'Thin layer approximation and algebraic model for separated turbulent flows', *AIAA Paper 78-257*, 1978.
6. S. C. Purohit, J. S. Shang and W. L. Hankey, 'Effect of suction on the wake structure of a three dimensional turret', *AIAA Paper 83–1738*, 1983.
7. F. E. Marble, 'Dynamics of dusty gases', *Ann. Rev. Fluid Mech.*, 397 (1970).
8. S. S. Gokhale and T. K. Bose, 'Reacting solid particles in one-dimensional nozzle flow', *Int. J. Multiphase Flow*, **15**, 269–278 (1989).
9. R. Peyret and H. Viviand, *Computational Methods for Fluid Flow*, Springer, New York, 1993, pp. 109–111.
10. A. Jameson, W. Schmidt and T. Turkel, 'Numerical solution of the Euler equations by finite volume methods using Runge–Kutta time-stepping schemes', *AIAA Paper 81-1259*, 1981.
11. R. F. Cuffel, L. H. Back and P. F. Massier, 'Transonic flow field in a supersonic nozzle with small throat radius of curvature', *AIAA J.*, **17**, 1364 (1969).